15 April 1999

ELSEVIER

Optics Communications 162 (1999) 347–356

OPTICS COMMUNICATIONS

Full length article

Dynamics of quadratic soliton excitation

David Artigas [a], Lluis Torner [a], Nail N. Akhmediev [b]

[a] *Laboratory of Photonics, Department of Signal Theory and Communications, Universitat Politecnica de Catalunya, Gran Capitan UPC-D3, ES 08034 Barcelona, Spain*

[b] *Optical Sciences Center, Institute of Advanced Studies, The Australian National University, Canberra, ACT 0200, Australia*

Received 2 December 1998; accepted 12 February 1999

Abstract

We study the dynamics of the soliton–radiation interaction in the process of soliton excitation in quadratic nonlinear media. The focus is on the dynamics of initial signals that are not weakly perturbed exact solitons. We use a combination of numerical experiments and analytical tools based on the integral conserved quantities of the wave evolution. We show the rate of convergence of representative, experimentally relevant inputs, to the asymptotic soliton states. A measure of soliton content of arbitrary input signals is introduced and evaluated in several representative examples. The dynamic evolution of oscillating solitons is studied using generalized Stokes parameters.

1. Introduction

Since their re-discovery a few years ago, quadratic solitons have been a subject of intense investigation [1,2]. Solitons have been observed experimentally in up and down conversion second-harmonic generation (SHG) and in parametric amplification schemes [3–8], and many of their basic properties are well established. In particular, families of spatial and temporal solitons existing in waveguides and in bulk geometries are known, including those existing in settings with a small Poynting vector walk-off and/or temporal group-velocity mismatch. Under conditions where modulational instabilities cannot grow, and with the exception of narrow regions near the cutoff conditions for soliton existence, such families of stationary solitons have been shown to be stable under propagation and robust against several perturbations.

Notwithstanding, the evolution equations used to model soliton formation in quadratic nonlinear media do not belong to that special class of equations, referred to as completely integrable, that have soliton solutions in the rigorous mathematical sense [9–11]. Therefore, except at the limit of large phase-mismatch between the several waves forming the quadratic solitons, where under appropriate conditions they can be treated as perturbed solitons of the nonlinear Schrödinger equation (NLSE), the tools and miracles that are exclusive of integrable systems do not hold. Naturally, this fact has important implications.

For example, contrary to integrable systems, the soliton content of an arbitrary signal, namely the fraction of the energy that corresponds to a soliton, is not known a priori. Also, collisions between several solitons and interactions between solitons and radiation are inelastic. Such features are intimately related, and are due to the friction, accompanied by energy exchange, that solitons experience when they interact with each other, and with linear waves. In particular, the interaction between solitons and linear waves manifests itself in the process of soliton excitation, or when exact stationary solitons are slightly perturbed, producing oscillating solitons. It is worth stressing that oscillations also appear in integrable systems, but in such case they appear only due to nonlinear interference between solitons and radiation, or between several solitons. Notice that in integrable systems the binding energy between solitons is zero.

In the case of quadratic solitons, an important point not always properly appreciated is that in the excitation of solitons with arbitrary inputs the shapes of the input signals are not necessarily close to those given by the soliton solutions of the governing equations. On the contrary, in the majority of cases, solitons are excited with inputs which fall very far from those solutions indeed. For

0030-4018/99/$ - see front matter
PII: S0030-4018(99)00088-7

example, such is the situation encountered when light at only one of the involved frequencies, namely the fundamental frequency (FF) or the second-harmonic (SH) when solitons are formed in SHG settings, is input to the crystal. Not so far, but in general still far from the stationary solitons are the conditions met when both, coherent but out-of-phase FF and SH signals are initially supplied, or in the single soliton formation through the inelastic collision and merging together of several initially separated solitons. In all such cases, the inputs ought to reshape and adjust themselves through radiation of dispersive waves to form a soliton. Intuitively, such inputs can be regarded as to contain the corresponding radiation together with the soliton that eventually emerges after the light propagation over an ideal infinite distance.

In this paper we report the salient points of the investigations performed to elucidate the interaction of solitons with radiation in the process of soliton excitation. The focus is on situations where the initial conditions are not close to the exact soliton shapes, so that the fraction of radiation contained in the input conditions is significant. We use a combination of numerical experiments and analytical tools based on the integral conserved quantities of the wave evolution. Our goal is to expose the rate of convergence of experimentally illustrative inputs, to the asymptotic soliton states. We introduce a measure of soliton content of arbitrary input signals and evaluate its value in several representative examples. We also examine the impact of radiation attached to oscillating solitons on their features.

The remainder of the paper is organized as follows. Section 2 contains the succinct formal statement of the problem addressed. In Sections 3 and 4 the governing equations, the integrals of the evolution, and the families of stationary, bright soliton solutions are presented. Section 5 is devoted to the excitation of solitons as monitored using energy-Hamiltonian diagrams. In Section 6 Stokes parameters are used to monitor the evolution of oscillating solitons, and in Section 6 we introduce a measure of soliton content. In Section 8 our main results are summarized.

2. Statement of the problem

Rigorous solitons of dynamical systems governed by completely integrable evolution equations enjoy unique features [9–11]. For our present purposes, we notice two salient points:

- *Existence of a spectral transform that gives the soliton content*, defined as the fraction of total energy that corresponds to a soliton, of an arbitrary input. For the NLSE, such soliton content is given by the eigenvalues of the Zakharov–Shabat scattering equations.
- *The soliton content remains constant during evolution.* Hence, collisions between several solitons and between solitons and dispersive waves, i.e. wave packets that considered alone carry a vanishing soliton content, ought to be elastic. Namely, without energy exchange.

For non-integrable systems, as is the case examined here, such features are lost. In particular, solitons interact with linear waves. Therefore, to the best of our knowledge, to date there is no known way to calculate the soliton content a priori or at intermediate stages of the propagation in the case of non-integrable systems. In what follows, we study the soliton–radiation interaction in the process of soliton excitation in the case of one-dimensional solitons that form in quadratic nonlinear media, and introduce an a posteriori measure of soliton content.

3. Governing equations

We focus here on spatial solitons formed in planar waveguides under conditions for type I SHG, but the analysis can be extended to higher-dimensional geometries, to temporal solitons, and to general three-wave mixing interactions. In the slowly-varying envelope approximation, the beam evolution can be described by the reduced equations [12]

$$i\frac{\partial a_1}{\partial \xi} - \frac{r}{2}\frac{\partial^2 a_1}{\partial s^2} + a_1^* a_2 \exp(-i\beta\xi) = 0,$$
$$i\frac{\partial a_2}{\partial \xi} - \frac{\alpha}{2}\frac{\partial^2 a_2}{\partial s^2} - i\delta\frac{\partial a_2}{\partial s} + a_1^2 \exp(i\beta\xi) = 0, \qquad (1)$$

where a_1 and a_2 are the normalized amplitudes of the FF and SH waves. In the case of spatial solitons $r = -1$ and $\alpha = -k_1/k_2$, where $k_{1,2}$ are the linear wave numbers at both frequencies. Actually, $\alpha \simeq -0.5$, so in the numerics we always set $\alpha = -0.5$. The transverse coordinate s is normalized to a beam width η, and the propagation coordinate ξ is normalized to the diffraction length at the FF ($l_{d1} = k_1\eta^2/2$). The parameter β is given by $\beta = k_1\eta^2\Delta k$, where $\Delta k = 2k_1 - k_2$ is the wave vector mismatch. The parameter δ accounts for the presence of Poynting vector walk-off that occurs in birefringent media when propagation is not along the crystal optical axes. Walk-off is absent in non-critical and usual quasi-phase-matching geometries. For our present purposes it is convenient to investigate configurations without walk-off, and we hereafter set $\delta = 0$. For a soliton width of about $\eta \sim 15$ μm that yields a diffraction length $l_{d1} \sim 1$ mm, ξ in the range 0–20, corresponds to a few cm.

Central to our approach in this paper is the fact that Eqs. (1) define an infinite-dimensional Hamiltonian system, with a conserved Hamiltonian that in the absence of walk-off is given by

$$H = -\tfrac{1}{2}\int\left[r\left|\frac{\partial A_1}{\partial s}\right|^2 + \frac{\alpha}{2}\left|\frac{\partial A_2}{\partial s}\right|^2 - \beta|A_2|^2 + A_1^{*2}A_2 + A_1^2A_2^*\right]\mathrm{d}s, \qquad (2)$$

where we have defined $A_1 = a_1$, and $A_2 = a_2 \exp(-i\beta\xi)$. The beam intensity or energy flow given by the Manley–Rowe relation

$$I = I_1 + I_2 = \int \left[|A_1|^2 + |A_2|^2 \right] \mathrm{d}s, \tag{3}$$

is also conserved. One finds that the stationary solitons of Eqs. (1) occur at the extrema of the Hamiltonian for a given energy flow. This is an important result that provides a powerful tool to analyze the dynamics of the wave evolution. We shall make use of such a tool shortly below.

4. Stationary solitons

The known stationary solutions of Eqs. (1) have the form $a_\nu = U_\nu(s)\exp(i\kappa_\nu \xi)$, where κ_ν, with $\kappa_2 = 2\kappa_1 + \beta$, are the nonlinear shifts of the wave numbers. The forms of U_1 and U_2 are given by the equations

$$\frac{r}{2}\frac{\mathrm{d}^2 U_1}{\mathrm{d}s^2} + \kappa_1 U_1 - U_1 U_2 = 0,$$

$$\frac{\alpha}{2}\frac{\mathrm{d}^2 U_2}{\mathrm{d}s^2} + (2\kappa_1 + \beta) U_2 - U_1^2 = 0. \tag{4}$$

Here r, α and β are given by material and linear wave parameters, while the nonlinear wave number shift κ_1 parametrizes the families of solitons. At present only the zero-parameter solution of Eqs. (4) given by [1,13,14]

$$U_1 = 3\mu\sqrt{\alpha r}\,\mathrm{sech}^2\sqrt{\mu}\,s, \quad U_2 = -3r\mu\,\mathrm{sech}^2\sqrt{\mu}\,s, \tag{5}$$

that holds at $\beta = -2\mu(\alpha - 2r)$, $\kappa_1 = -2r\mu$, with $\mu > 0$ being a free scaling parameter, is known in analytical form. The whole families were found numerically [15,16]. Useful approximate expressions can also be obtained by using variational methods [17]. Central to our analysis here is the relation between the energy flow and the Hamiltonian of the solutions. One finds that the one-dimensional solutions occur at $H = -\frac{3}{5}\kappa_1 I + \frac{1}{5}\beta I_2$. Thus, the curve $H(I)$ has to be calculated numerically. Figs. 1–4 show the outcome of the calculations at positive and negative wave vector mismatches, and at exact phase-matching [18]. At $\beta = 0$ one can use the similarity rules of Eqs. (4) to obtain $H_{\beta=0} = -\frac{3}{5} c_1 I^{5/3}$, where c_1 is a constant. Numerically, one finds $c_1 \simeq 0.206$.

5. Soliton excitation

As mentioned above, the stable stationary solutions realize the absolute minimum of H for each I. Therefore, to monitor the dynamics of the evolution of arbitrary input conditions, one can compute the values of the Hamiltonian and energy flow in a window of finite width centered at the peak of the evolving localized fields, which shall be referred as $\tilde{H}(\xi)$ and $\tilde{I}(\xi)$, and plot their evolution in the corresponding $H(I)$ diagram. Explicitly,

$$\tilde{I}(\xi) = \int_{s_p - L}^{s_p + L} i(\xi, s)\,\mathrm{d}s, \tag{6}$$

where s_p is the position of the soliton peak, $2L$ is the width of a suitable calculation window, and $i(s)$ is the energy flow density. An analogous expression holds for $\tilde{H}$. The length L can be chosen to be a few soliton widths, so that the calculation window contains all the soliton integrals up to the desired numerical accuracy. An input that does not coincide with a stationary solution either spreads or it reshapes and radiates energy away and eventually excites a stable stationary soliton. In the first case, $\tilde{H}(\infty) = 0$, $\tilde{I}(\infty) = 0$, whereas in the second situation $\tilde{H}(\xi)$ and $\tilde{I}(\xi)$ approach one point of the curve corresponding to the stationary solutions. On intuitive grounds, the trajectory from the initial to the final point of the $H(I)$ diagram, and the rate of convergence, can be viewed as dictated by the interaction between the soliton, defined as the soliton that is eventually excited, and the radiation that hence can be viewed as being attached to it.

We examined initial conditions with different shapes, peak amplitudes and relative global phases of the FF and SH signals, with the general form: $a_1(\xi = 0, s) = A\,\mathrm{sech}^a(s)$, $a_2(\xi = 0, s) = B\,\mathrm{sech}^b(s)\exp(i\phi_0)$. Importantly, notice that the width of such fields is fixed. Because of the form of the analytical solution (5), in all the results shown through the paper corresponding to $\beta \le 0$ we set $a = b = 2$. Then, the input conditions correspond to the point of the I–H diagram given by

$$H = \tfrac{2}{15}\left[4A^2 + (5\beta + 1)B^2 - 8A^2 B\cos(\phi_0)\right], \tag{7}$$

$$I = \tfrac{4}{3}(A^2 + B^2). \tag{8}$$

In some of the results presented for $\beta > 0$ we set $a = 1$ and $b = 2$. Then, the initial conditions correspond to the point of the I–H diagram given by

$$H = \tfrac{1}{3}\left[A^2 + \left(2\beta + \tfrac{2}{5}\right)B^2 - 4A^2 B\cos(\phi_0)\right], \tag{9}$$

$$I = 2\left(A^2 + \tfrac{2}{3}B^2\right). \tag{10}$$

At $\beta > 0$ we frequently consider that no SH light is present at the input, so that then the initial conditions become $H = A^2/3$ and $I = 2A^2$.

We start with the latter case and $\beta = 10$. Fig. 1 shows the trajectories followed by input conditions with increasing energy in the corresponding I–H diagram. As discussed below in Section 7 for such inputs there is a minimum threshold value of the input peak amplitude for the excitation of solitons, even though all the cases shown in the plot correspond to conditions above such threshold. First, we examine the rate of convergence to the asymptotic soliton states. The full triangles and open circles shown for each trajectory indicate the points reached at the

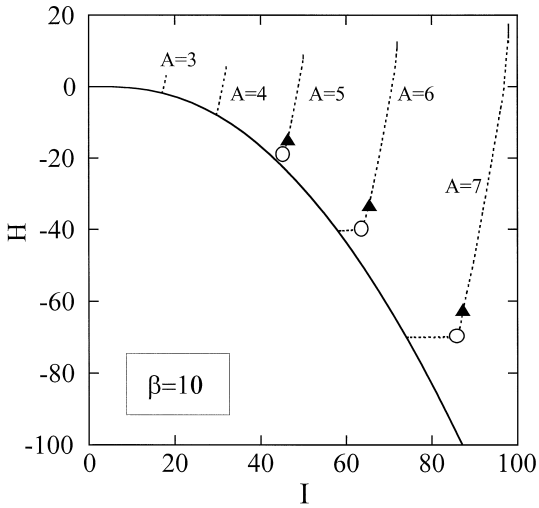

Fig. 1. Evolution of several input conditions, and families of stationary solitons represented in energy flow-Hamiltonian diagrams. Solid lines: families of stationary solitons; dashed lines: ''trajectories'' followed during propagation. Positive wave vector mismatch ($\beta = 10$). Input conditions: $B = 0$, $a = 1$, and labels indicate the value of A. Full triangles: location at $\xi = 10$; open circles: $\xi = 20$. Under typical experimental conditions for spatial soliton formation with widths of 10–20 μm the normalized distance $\xi = 20$ corresponds to a crystal length of about 4 cm.

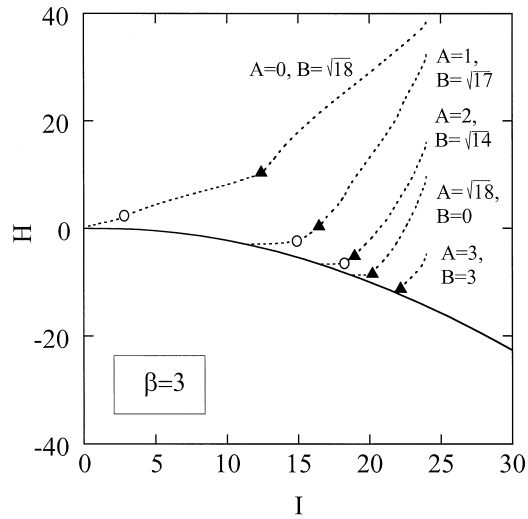

Fig. 2. Analogous to Fig. 1, but nearer phase-matching ($\beta = 3$). Input conditions: $a = 2$, $b = 2$, $\phi_0 = 0$, and labels indicate the values of A and B.

propagation distances $\xi = 10$ and $\xi = 20$, respectively. Naturally, the exact location of such points depends slightly on the width of the numerical window chosen to calculate the values of I and H around the soliton. However, for judicious choices of such a width the differences are not even visible in the plots. The first conclusion to the raised from Fig. 1 is that under the conditions of the plot, namely reasonably large positive wave vector mismatch and moderate input energies, the inputs converge fast to the final soliton state. This is because under such conditions the beam evolution can be viewed as given by a perturbed NLSE for the FF wave [12]. The curves corresponding to the input peak amplitudes $A = 6$ and $A = 7$ reveal a new feature, that we only observed to occur with large positive values of β. Namely, an abrupt change of behavior at a given propagation distance. During the first propagation units, the fields reshape fast so that the Hamiltonian of the evolving fields decreases rapidly, but after that the evolution takes place with almost constant Hamiltonian.

Figs. 2 and 3 show the typical evolution at a small positive phase-mismatch ($\beta = 3$) and at exact phase-matching ($\beta = 0$), respectively. The plots show the evolution of various inputs with identical energy flow but different features, in terms of relative peak amplitudes and phases of the FF and SH waves. In Fig. 2 the FF and SH inputs are in-phase, but have different peak amplitudes. In Fig. 3 the amplitudes of the inputs are $A = B = 3$ in all cases, and the various input conditions correspond to different values of the relative global phase ϕ_0. When the input conditions fall close to the curve corresponding to the exact family of stationary solitons the input excite a soliton. However, the point shown in Figs. 2, 3 is that even though in all cases the input energy is far above the threshold required for soliton formation, when such energy is not properly supplied, the beams spread. In particular, Fig. 3 illustrates the situation encountered in practice when solitons are intended to be formed supplying both a FF wave and a coherent but out-of-phase SH seed at the input

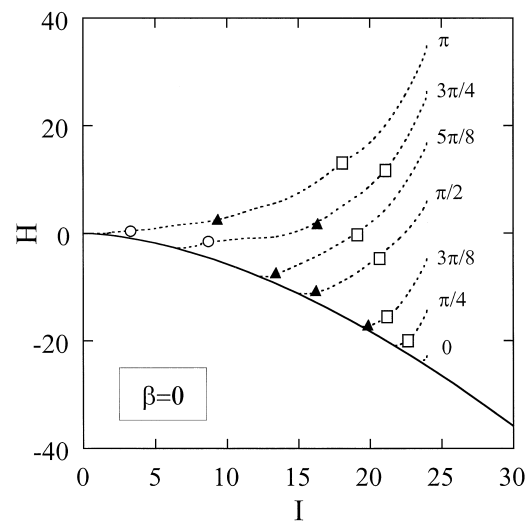

Fig. 3. Analogous to Fig. 1, but at exact phase-matching ($\beta = 0$). Input conditions: $a = 2$, $b = 2$, $A = 3$, $B = 3$, and labels indicate the value of ϕ_0. Open squares: location at $\xi = 5$, full triangles: $\xi = 10$; open circles: $\xi = 20$.

of the quadratic crystal. The plots show that the relative phases between the signals strongly impact the fraction of the input energy that is eventually carried by the excited soliton. For example, with in-phase signals the soliton formed carries almost all the input energy, whereas when $\phi_0 = \pi$, solitons are not formed, so that all the energy spreads in the form of radiation.

The evolution of arbitrary inputs at negative β is more complicated. Fig. 4 shows a few representative examples. Here the open circles and triangles shown for each trajectory indicate the points reached at the propagation distances $\xi = 20$ and $\xi = 50$, respectively. Recall that for the typical conditions met in the experimental formation of spatial solitons with widths of some 10–20 μm, the normalized distance $\xi = 50$ would already correspond to a theoretical crystal length larger than 10 cm. To stress the differences between the dynamical regime explored here and that considered in previous works where the evolution of weakly perturbed exact solutions was studied, the evolution from point labeled E in Fig. 4 corresponds to the input conditions considered by Etrich et al. [20], in the case of the perturbed analytical solution (5) with the amplitude perturbation, as defined in Eq. (2) of Ref. [20], equal to 0.25, which is the largest perturbation amplitude allowed to avoid phase dislocations across the transverse axis. The drastic difference in the input conditions considered is clearly visible.

First, Fig. 4 shows that by and large the rate of convergence of the inputs towards the asymptotic steady state is much slower than at $\beta > 0$. This is because of the stronger interaction between solitons and radiation, manifested by the excitation of the so-called soliton ''internal modes'', at negative β. We will return to this point in the next section. Fig. 4 also illustrates that even though different initial conditions can correspond to the same point of the I–H diagram, as it is the case for the two conditions $\{A = 3,\ B = 3,\ \cos(\phi_0) = -1/27\}$ and $\{A = \sqrt{17},\ B = 1,\ \phi_0 = 0\}$ shown, their evolution is different thus so is the soliton excited. The evolution of the input with $\{A = 3,\ B = 3,\ \phi_0 = 5\pi/8\}$ shows the excitation of one of the ''quasi-bound modes'' discovered in Ref. [20]. The mode shown exists for an energy below the threshold for stationary soliton existence. The fields radiate energy while their trajectory tends to the $I = 0$, $H = 0$ point. Yet, such leak is extremely small, hardly distinguishable from the accuracy of the numerical scheme. For the particular conditions considered in Fig. 4 we observed excitation of such modes with inputs having $H \approx 0$. For clearly positive values of H, such as for $\{A = 3,\ B = 3,\ \phi_0 = \pi\}$, the beams spread.

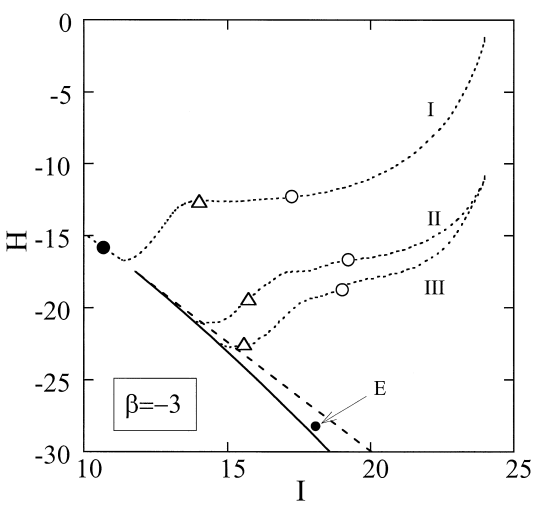

Fig. 4. Analogous to Fig. 1, but at a small negative wave vector mismatch ($\beta = -3$). I: $A = 3$, $B = 3$, $\phi_0 = 5\pi/8$; II: $A = \sqrt{17}$, $B = 1$, $\phi_0 = 0$; III: $A = 3$, $B = 3$, $\cos(\phi_0) = -1/27$. In all cases: $a = 2$, $b = 2$. Open circles: location at $\xi = 20$; open triangles: $\xi = 50$; big full dot: $\xi = 10^5$. Point labeled E corresponds to a weakly perturbed analytical solution considered in Ref. [20] (see text for details). Solid curve: family of stable solitons; long-dashed curve: unstable solutions.

6. Oscillating solitons

The trajectories followed by the evolving signals in the I–H diagrams shown in Figs. 1–4 give important, but only partial information about the wave evolution. For example, in Fig. 4 the evolving signals seem to ''cross'' the family of unstable solutions, but such is not necessarily the case because the evolution takes place in an infinite-dimensional space, while I–H diagrams are only two-dimensional. Also, by and large the convergence of the input conditions to the asymptotic steady states reached at $\xi \to \infty$ shown in Figs. 1–4 takes place through the generation of ''oscillating solitons''. Such oscillations can be very persistent but they are not visible in the above trajectories, except for the fact that they make the convergence rate very slow.

To gain further insight into the dynamics of the wave evolution we introduce generalized differential Stokes parameters defined as

$$S_0(\xi, s) = |A_1|^2 + |A_2|^2, \tag{11}$$

$$S_1(\xi, s) = |A_1|^2 - |A_2|^2, \tag{12}$$

$$S_2(\xi, s) = \frac{1}{|A_1|}\left[A_1^2 A_2^* + A_1^{*2} A_2\right], \tag{13}$$

$$S_3(\xi, s) = \frac{1}{|A_1|}\left[A_1^2 A_2^* - A_1^{*2} A_2\right], \tag{14}$$

which verify

$$S_1^2 + S_2^2 + S_3^2 = S_0^2. \tag{15}$$

Writing general fields in the form $A_\nu(\xi,s) = R_\nu(\xi,s)\exp[i\phi_\nu(\xi,s)]$, with R_ν and ϕ_ν being real functions, one has

$$S_0 = R_1^2 + R_2^2, \tag{16}$$

$$S_1 = R_1^2 - R_2^2, \tag{17}$$

$$S_2 = 2R_1R_2\cos(2\phi_1 - \phi_2), \tag{18}$$

$$S_3 = 2R_1R_2\sin(2\phi_1 - \phi_2). \tag{19}$$

The stationary soliton solutions verify $\phi_1 = \kappa_1$, $\phi_2 = \kappa_2 - \beta$, which leads to $S_3 = 0$. We are interested in the evolution of the generalized differential Stokes parameters evaluated at the soliton peak, namely $s_m(\xi) = S_m(\xi, s = 0)$, $m = 0 - 3$. The parameters s_1–s_2–s_3 evolve in a Poincaré sphere of radius s_0, but the value of s_0 changes dynamically due to the emission of radiation from the solitons. For some purposes it might be useful to monitor the evolution of the parameters scaled to s_0, but to make the radiative effects visible here we do not proceed that way. Rather, we evaluate the four s_m parameters and monitor their dynamical evolution by plotting their trajectories in suitable two-dimensional representations.

The sketch displayed in Fig. 5 shows the loci of the families of stationary soliton solutions in the s_1–s_2–s_3 space, together with a few illustrative excitation points. The most symmetric excitation conditions are located along either of the axes. The families of stationary solutions are located at the plane s_1–s_2 indeed. Because at $\beta = 0$ all the stationary solutions are self-similar, they are located at the straight line

$$\frac{s_2}{s_1} = c_a, \quad \text{with } s_0 = c_b\, I^{4/3}, \tag{20}$$

where c_a and c_b are numerical constants. One finds $c_a \simeq 5.286$, and $c_b \simeq 0.297$. At $\beta > 0$ the cut-off point for soliton existence, given by $\kappa_1 = 0$, is located at the origin $(s_1,s_2) = (0,0)$. At $\beta < 0$ cut-off occurs at $\kappa_2 = 0$, yielding the point $(-\beta^2/4,0)$. The locus of the zero-parameter analytical solution given by expression (5) at $\beta < 0$ is located at

$$s_1 = -\tfrac{1}{2}\beta^2, \quad s_2 = \sqrt{2}\,\beta^2, \tag{21}$$

with

$$s_0 = \tfrac{3}{2}\beta^2. \tag{22}$$

The diagram that is obtained using the scaled parameters $\tilde{s}_n = s_n/s_0$, $n = 1$–3, is shown in the sketches of Fig. 6. The arrows appearing in the drawing indicate the direction of increasing soliton energy. In this more compact representation, all stationary solutions existing at $\beta = 0$ are located at a single point, numerically given by $(\tilde{s}_1,\tilde{s}_2) \simeq (0.186,0.983)$, cut-off occurs at the points $(1,0)$ at $\beta > 0$, and $(-1,0)$ at $\beta < 0$, and the zero-parameter analytical solution (5) is located at the point $(-1/3,2\sqrt{2}/3)$.

The plots shown in Figs. 7 and 8 illustrate the typical evolution as seen using the non-scaled Stokes parameters, in the two representative cases. The families of stationary solutions, which are all located in the $s_3 = 0$ plane, are also shown. In Fig. 7, the excitation conditions correspond to the points labeled E1 and E2 in Fig. 5, and in both cases $\beta = -3$, $A = 4$, and $B = 4$, but for E1 one has $\phi_0 = \pi$, whereas E2 corresponds to $\phi_0 = \pi/8$. As shown in Fig. 7(a), the input conditions E1 spread, thus all the non-scaled

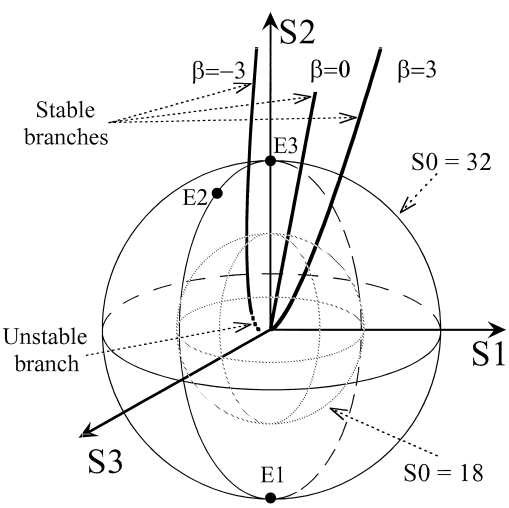

Fig. 5. Sketch of the Poincaré sphere defined by the generalized Stokes parameters showing the loci of the families of soliton solutions for different values of β, together with a few excitation points (labeled E1–E3) whose evolution is shown in Figs. 7 and 8. The spheres drawn with radius $s_0 = 18$ and $s_0 = 32$ correspond to the inputs of Figs. 2–4 and Figs. 7, 8, respectively.

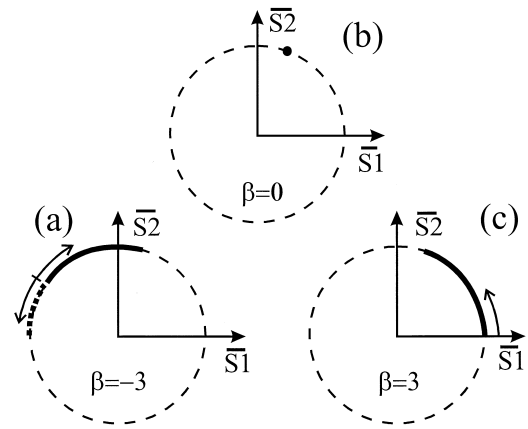

Fig. 6. Sketch showing the loci of the families of stationary soliton solutions existing for different values of β represented using the scaled Stokes parameters. The arrows indicate the direction of increasing soliton energy.

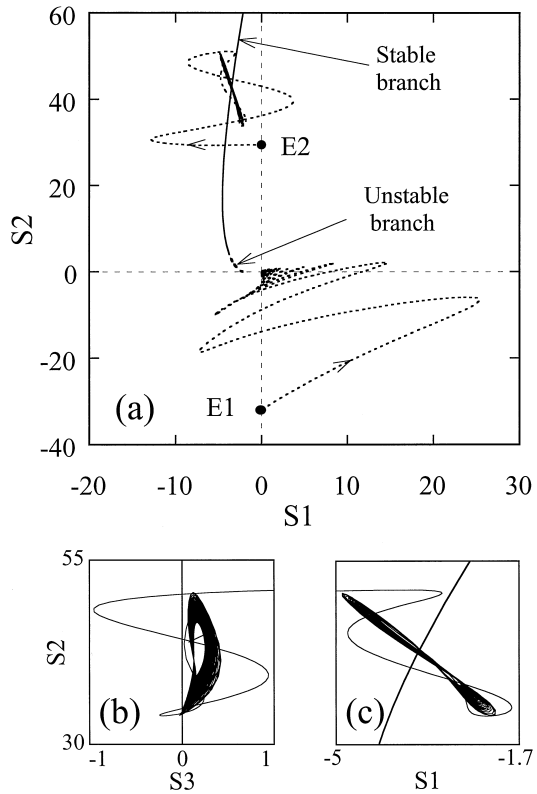

Fig. 7. Evolution of the excitation points E1 and E2 of Fig. 5. Normalized wave vector mismatch $\beta = -3$. E1 spreads; E2 excites an oscillating soliton. Input conditions: $a = 2$, $b = 2$, $A = 4$, $B = 4$. For E1: $\phi_0 = \pi$; for E2: $\phi_0 = \pi/8$. The plots show the evolution until $\xi = 200$.

Stokes parameters s_m converge to the origin. Physically, with $\phi_0 = \pi$ the provoked energy exchange between the FF and SH waves prevents the formation of solitons. Geometrically, such difficulty is manifested by the fact that the excitation conditions E1 belong to the lower semi-space $s_2 < 0$ while the soliton states lay far, in the upper semi-space.

The input conditions corresponding to E2 reshape and excite a soliton. The dynamics of the evolution is more visible in the zooms displayed in Figs. 7(b) and 7(c). Such plots show that the FF and SH waves are locked both, in amplitude and in phase. After the initial reshaping, the evolution towards the asymptotic soliton state is extremely slow. In Fig. 7 the evolution is shown until $\xi = 200$, but no significant differences were observed when the propagation distance was increased several orders of magnitude. The plots clearly stress the oscillating nature of the corresponding solitons [19].

The oscillations are due to the soliton interaction with the radiation present and to the excitation of a so-called soliton ''internal mode'' [20–22]. In the case of quadratic solitons, internal modes have been shown to exist only for given ranges of wave vector mismatches and soliton energies [20]. When they are absent, as in the evolutions shown, e.g., in Figs. 1 and 2, the input conditions shed most of the radiation away during the first tens of propagation units and then converge fast to the stationary soliton states. To allow direct comparison with Fig. 7, a typical example of such evolution as seen using the generalized Stokes representation is shown in Fig. 8. However, under the conditions where internal modes exist, the oscillations are extremely persistent. Recent perturbative investigations reported in Ref. [22] appear to suggest that at large distances the radiation is emitted at a logarithmic rate, and we indeed had found numerically that the oscillations persist beyond one million propagation units (i.e., $\xi > 10^6$) exhibiting decay rates hardly distinguishable from the actual accuracy of the numerical scheme.

Fig. 7(a) shows another important feature. Namely, the fact that even though in the I–H diagram, many excitation conditions (e.g., E2) during their dynamical evolution seem to ''cross'' over the family of unstable stationary solutions arising near the cut-off for soliton existence, such is not the case indeed. Therefore, such unstable solutions have a very limited relevance to the experimental excitation of solitons.

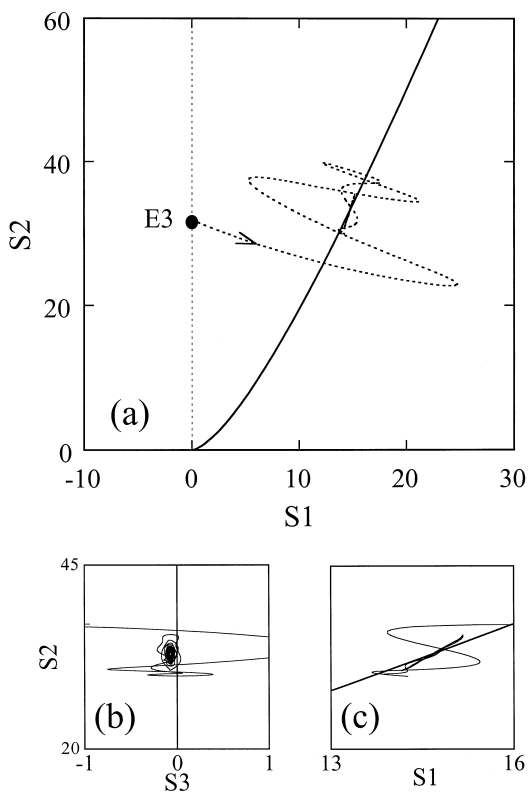

Fig. 8. Analogous to Fig. 7, but at positive wave vector mismatch ($\beta = 3$). Input conditions: $a = 2$, $b = 2$, $A = 4$, $B = 4$, $\phi_0 = 0$.

There are a large variety of excitation conditions whose evolution can be usefully monitored using the above representation. In general, analogous qualitative features as those shown in Figs. 7, 8 are obtained. Thus, we devote the remainder of the paper to study a new feature, that can be viewed as the measure of the efficiency of the process of soliton excitation. Namely, the fraction of input energy that is captured by the excited soliton.

7. Soliton content

We restrict to input conditions at which at most only one soliton is formed. In such case, one can define the single soliton content (SSC) of an arbitrary input as the fraction of the input energy that is carried by the soliton that is eventually excited. Namely,

$$\mathrm{SSC} = \frac{I_{\mathrm{soliton}}}{I_{\mathrm{input}}}. \tag{23}$$

When the input does not excite a soliton one has SSC = 0, and when the input is an exact, stable soliton solution of the governing equations SSC = 1. Otherwise, $0 < \mathrm{SSC} < 1$.

As mentioned above, in the case of dynamical systems governed by completely integrable evolution equations the SSC is a constant of the evolution. Hence, it can be calculated at any instance of the propagation, and in particular at $\xi = 0$, using the corresponding Lax pair of the system. For example, in the case of the NLSE one has

$$\mathrm{SSC} = \frac{2\eta}{I_{\mathrm{input}}}, \tag{24}$$

where η is given by the imaginary part of the eigenvalue of the Zakharov–Shabat scattering equations calculated for the input conditions or at any instance of the evolution. The details of the procedure are particularly well described in Ref. [9]. For weakly perturbed integrable systems an intuitive measure of soliton content can still be obtained by monitoring the evolution of the eigenvalues of the corresponding Lax pair. Relevant examples include a variety of perturbed NLSEs [23–30], and also quadratic solitons under appropriate conditions far from phase-matching [31,32]. However, for non-integrable evolution equations as it is the case of (1), to date a precise definition of soliton content can only be given a posteriori. In other words, SSC can only be calculated at $\xi \to \infty$. Namely,

$$\mathrm{SSC} = \frac{1}{I_{\mathrm{input}}} \lim_{\xi \to \infty} \tilde{I}(\xi), \tag{25}$$

where $\tilde{I}(\xi)$ is given by (6).

We have evaluated such soliton content for several illustrative examples. Fig. 9 shows the soliton content obtained at $\beta = 10$ and $\beta = 3$ when the input comprises only light at the FF with the form $a_1(\xi = 0, s) = A\,\mathrm{sech}(s)$, as a function of the input peak amplitude A. The dotted lines are the estimates for such inputs calculated using the Zakharov–Shabat scattering equations associated to the NLSE that is obtained from (1) when $\beta \gg 1$ and conversion to the SH is negligible. One gets

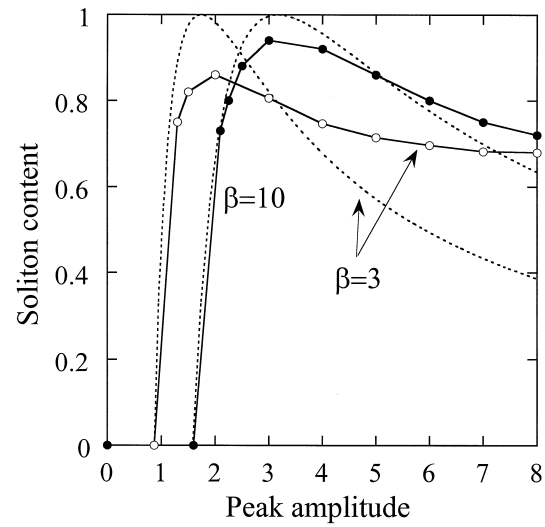

Fig. 9. Soliton content at positive wave vector mismach for sech-like FF signals ($a = 1$), as a function of the input peak amplitude A. No initial SH ($B = 0$). Labels indicate the value of β. Discrete points are the results of numerical experiments, the solid lines are only to help the eye. Dotted lines are estimates from the limiting NLSE.

$$\mathrm{SSC}_{\mathrm{NLSE}} = \frac{\sqrt{\beta}}{A^2}\left(2A - \sqrt{\beta}\right), \tag{26}$$

for $A \geq \sqrt{\beta}/2$. The plot reveals that there is a minimum peak amplitude below which the soliton content vanishes, thus the signals spread, and there is an optimum input peak amplitude at which the soliton content reaches its maximum value. Such critical peak amplitudes, as well as the value of the maximum soliton content, depend on the value of β. At $\beta > 0$, the threshold input FF peak amplitude for soliton formation is given by the NLSE limiting value $A_{\mathrm{th}} = 0.5\sqrt{\beta}$. At $\beta \gg 1$, the limiting NLSE predicts that the maximum soliton content, which for the ideal NLSE would be $SSC \simeq 1$, is reached with $A_m \simeq \sqrt{\beta}$. Fig. 9 shows that at $\beta = 10$ such expression gives a good estimate of the actual value and even at $\beta = 3$ it gives an useful approximation.

One observes that the maximum value of the SSC is smaller at $\beta = 3$ than at $\beta = 10$. This is because the shape of the input signals differ a larger extent from the corresponding soliton families, mainly because for a given soliton energy, as β decreases the fraction of energy carried by the SH wave (which is not initially supplied) increases.

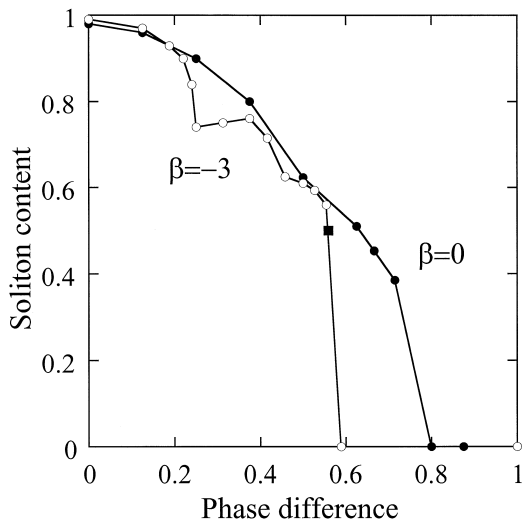

Fig. 10. Analogous to Fig. 9, but at exact phase-matching and at negative wave vector mismach and for input conditions with $a = 2$, $b = 2$, $A = 3$ and $B = 3$, as a function of the phase difference ϕ_0 between the FF and SH input signals. Labels indicate the value of β. Full square: minimum non-vanishing soliton content possible at $\beta = -3$ for inputs with $I = 24$, numerically equal to ≈ 0.49.

Fig. 10 shows the soliton content calculated at $\beta = 0$ and at $\beta = -3$ with the input conditions $a_1(\xi = 0, s) = A\,\mathrm{sech}^2(s)$, $a_2(\xi = 0, s) = B\,\mathrm{sech}^2(s)\exp(i\phi_0)$, with $A = B = 3$ in all cases, as a function of the global phase ϕ_0. In agreement with Figs. 3 and 4, the soliton content is found to decrease with increasing de-phasing, even though not necessarily monotonically as shown by the curve corresponding to $\beta = -3$.

Important information can be obtained from curves of soliton content for a variety of input conditions that was not possible to examine here. For example, in the case of two-dimensional (i.e., $(2 + 1)$) solitons propagating in bulk crystals, curves of soliton content as a function of wave vector mismatch, input power or beam ellipticity have direct applications to the design of soliton devices for optical beam clean-up [33], and for bandwidth-enhancement in second-harmonic generation schemes [34].

8. Concluding remarks

To summarize, we have studied the dynamics of the excitation of quadratic solitons from input conditions that contain a significant amount of energy that is gradually radiated away. Our goal was to target two crucial features on regard to soliton formation: The soliton content, or fraction of the input energy flow that is captured by the excited soliton, and the rate of convergence of the input light signal to the asymptotic soliton states.

We have shown that a great deal of the important information about the process can be exposed by monitoring the wave evolution using energy flow-Hamiltonian diagrams and generalized Stokes parameters. The outcome stresses the oscillating nature of many quadratic solitons when they are excited with realistic input signals. A measure of soliton content of arbitrary inputs has been introduced and evaluated in several illustrative examples. Such calculations revealed, in particular, that with only fundamental input light the soliton content exhibits a maximum at a finite input peak amplitude. Thus, increasing the input energy does not necessarily lead to a larger soliton content. The optimum input peak amplitude and maximum soliton content attainable have been shown to depend, in particular, on the existing wave vector mismatch. Eventually, we emphasize that the approach discussed has applications to soliton excitation in analogous but different settings modeled by non-integrable evolution equations.

Acknowledgements

This work has been supported by the Spanish Government under contract PB95 0768. The numerical work has been carried out at the C^4-Centre de Computacio i Comunicacions de Catalunya. N.N. Akhmediev is at the Australian Photonics Cooperative Research Centre.

References

[1] Yu.N. Karamzin, A.P. Sukhorukov, Sov. Phys. JETP 41 (1976) 414.
[2] For reviews, see G.I. Stegeman, D.J. Hagan, L. Torner, Opt. Quantum Electron. 28 (1996) 1691; L. Torner, in: F. Kajzar, R. Reinisch (Eds.), Beam Shaping and Control with Nonlinear Optics, Plenum, New York, 1998, pp. 229–258.
[3] W.E. Torruellas, Z. Wang, D.J. Hagan, E.W. VanStryland, G.I. Stegeman, L. Torner, C.R. Menyuk, Phys. Rev. Lett. 74 (1995) 5036.
[4] R. Schiek, Y. Baek, G.I. Stegeman, Phys. Rev. E 53 (1996) 1138.
[5] M.T.G. Canva, R.A. Fuerst, D.M. Baboiu, G.I. Stegeman, G. Assanto, Optics Lett. 22 (1997) 1683.
[6] R.A. Fuerst, M.T.G. Canva, D.M. Baboiu, G.I. Stegeman, Optics Lett. 22 (1997) 1749.
[7] P. Di Trapani, G. Valiulis, W. Chinaglia, A. Andreoti, Phys. Rev. Lett. 80 (1998) 265.
[8] P. Di Trapani, D. Caironi, G. Valiulis, A. Dubietis, R. Danielius, A. Piskarskas, Phys. Rev. Lett. 81 (1998) 570.
[9] G.L. Lamb Jr., Elements of Soliton Theory, Wiley, New York, 1980.
[10] A. Hasegawa, Y. Kodama, Solitons in Optical Communications, Clarendon, Oxford, 1995.
[11] N.N. Akhmediev, A. Ankiewicz, Solitons, Chapman and Hall, London, 1997.
[12] C.R. Menyuk, R. Schiek, L. Torner, J. Opt. Soc. Am. B 11 (1994) 2434.

[13] M.J. Werner, P.D. Drummond, J. Opt. Soc. Am. B 10 (1993) 2390.
[14] K. Hayata, M. Koshiba, Phys. Rev. Lett. 71 (1993) 3275.
[15] A.V. Buryak, Y.S. Kivshar, Phys. Lett. A 197 (1995) 407.
[16] L. Torner, Optics Comm. 114 (1995) 136.
[17] V.V. Steblina, Y.S. Kivshar, M. Lisak, B.A. Malomed, Optics Comm. 118 (1995) 345.
[18] L. Torner, D. Mihalache, D. Mazilu, N.N. Akhmediev, Optics Lett. 20 (1995) 2183.
[19] L. Torner, C.R. Menyuk, G.I. Stegeman, J. Opt. Soc. Am. B 12 (1995) 889; L. Torner, E.M. Wright, J. Opt. Soc. Am. B 13 (1996) 864.
[20] C. Etrich, U. Peschel, F. Lederer, B.A. Malomed, Y.S. Kivshar, Phys. Rev. E 54 (1996) 4321.
[21] Y.S. Kivshar, D.E. Pelinovsky, T. Cretegny, M. Peyrard, Phys. Rev. Lett. 80 (1998) 5032.
[22] D.E. Pelinovsky, Y.S. Kivshar, V.V. Afanasjev, Physica D 116 (1998) 121.
[23] K.J. Blow, D. Wood, Optics Comm. 58 (1986) 349.
[24] K.J. Blow, N.J. Doran, in: J.R. Taylor (Ed.), Optical Solitons: Theory and Experiment, Cambridge University Press, 1992, pp. 73–106.
[25] S.R. Friberg, K.W. DeLong, Optics Lett. 17 (1992) 979.
[26] A. Hasegawa, T. Nyu, J. Lightwave Technol. LT-11 (1993) 395.
[27] R.J. Hawkins, C.R. Menyuk, Optics Lett. 23 (1993) 1999.
[28] V.V. Afanasjev, J.S. Aitchison, Y.S. Kivshar, Optics Comm. 116 (1995) 331.
[29] D. Artigas, L. Torner, J.P. Torres, N.N. Akhmediev, Optics Comm. 143 (1997) 322.
[30] M. Gölles, I.M. Uzunov, F. Lederer, Phys. Lett. A 231 (1997) 195.
[31] L. Torner, J.P. Torres, C.R. Menyuk, Optics Lett. 21 (1996) 464.
[32] J.P. Torres, L. Torner, Opt. Quantum Electron. 29 (1997) 757.
[33] R.A. Fuerst, B.L. Lawrence, W.E. Torruellas, G. I Stegeman, Optics Lett. 22 (1997) 19.
[34] M. Ohkawa, R.A. Fuerst, G.I. Stegeman, J. Opt. Soc. Am. B 15 (1998) 2769.